Journal of Solid State Chemistry **163,** 459–465 (2002)
doi:10.1006/jssc.2001.9426, available online at http://www.idealibrary.com on IDEAL®

Influence of Grain Size, Oxygen Stoichiometry, and Synthesis Conditions on the γ-Fe_2O_3 Vacancies Ordering and Lattice Parameters

T. Belin, N. Guigue-Millot, T. Caillot, D. Aymes, and J. C. Niepce

Laboratoire de Recherches sur la Réactivité des Solides, UMR 5613 Université de Bourgogne-CNRS, BP 47870, 21078 Dijon cedex, France

Received July 13, 2001; in revised form September 26, 2001; accepted October 5, 2001; published online December 21, 2001

The soft chemistry method has been used to synthesize γ-Fe_2O_3 nanoparticles: various synthesis temperature were applied to obtain nanometric powders with crystallite size in the 9–14 nm range. Powders were characterized by X-ray diffraction (XRD), Fourier transform infrared (FT-IR) spectrophotometry, surface area measurements, and electron microscopy (TEM, SEM). It is clearly shown that these nanometric powders are very well crystallized as indicated by XRD and IR spectra which present substructural bands attributed to vacancies ordering ($P4_132$). Based on these model materials and in the crystallite size range studied here, cell parameter appears to be not linked to crystallite size. It rather depends both on hydroxide adsorption and chemical composition. © 2002 Elsevier Science (USA)

Key Words: **maghemite; soft chemistry; nanometric crystallites; X-ray diffraction; surface.**

1. INTRODUCTION

The physical properties of nanosized materials exhibit substantial differences from those of micrometric materials (1). With decreasing particle size, an increasing fraction of atoms lies near or on the surface. Moreover, the intrinsic properties are strongly influenced by the surface in the nanometric scale. Indeed, the surface represents the interface between a solid and its environment. Since the solid interacts only through this interface with its surroundings, surface properties are of general interest. For example in catalysis, the effect of chemisorption on surface electronic properties has been checked (2). The surface effect could be explained via two parameters: the surface stress coming from the volume/surface discontinuity, which will influence the properties of materials, and the surface energy, induced by the creation of free chemical bonds near the surface, which will disturb the thermodynamical properties of materials. For example, several studies have been reported in the literature about the lattice parameter dependence on the average crystallite size. This dependence has been shown for γ-Fe_2O_3 powders (1) and for $BaTiO_3$ samples (3–5). To explain this experimental relationship, the Laplace law has been introduced. The relationship between lattice parameter and crystallite size has been explained by surface influence. Since the surface energy is positive, the original Laplace law implies that the internal pressure in the crystallite is more important in fine crystallites than in coarse ones. Therefore, a lattice parameter decrease would be observed when crystallite size decreases. Since the opposite is observed, a derived Laplace law which introduce surface stress (T_s) instead of surface energy has been developed by P. Perriat to take care of $BaTiO_3$ properties in fine powders (6, 7): for crystallite size smaller than 0.08 μm, the material is cubic and the smaller the crystallite size, the greater the cell parameter. This derived Laplace law $P_{int} = P_{ext} + 4T_s/D$ gives the internal pressure, P_{int}, as a function of both the external pressure P_{ext} and the surface stress per unit area. With this model, the cell parameter in the crystallite can decrease (when T_s is positive) or increase (when T_s is negative) when crystallite size decreases. Nevertheless, the surface stress necessary to explain the experimental lattice parameter variation with grain size is prohibitive ($>10\ J{\cdot}m^{-2}$). So new explanations have to be sought (such as noncontrolled parameters: adsorption, stoichiometry…). Iron oxides which play a key role in several important processes have been chosen for this new study.

The crystalline structure of most of the iron oxide can be described in terms of close-packed planes of O^{2-} anions with Fe cations occupying the interstitial octahedral and, in some cases, tetrahedral sublattices. Often both hexagonal and cubic polymorphs exist (8). Maghemite γ-Fe_2O_3, the ferrimagnetic cubic form of Fe(III) oxide is closely related to the structure of inverse spinel Fe_3O_4 but differs from the latter by the presence of vacancies distributed on the cation sublattice. Its formula can be written $(Fe^{3+})[Fe^{3+}_{5/3}\square_{1/3}]O_4$ where ( ) and [ ] designate respectively tetrahedral and octahedral coordination. It has been suggested that the vacancies can be distributed at random (space ground $Fd\bar{3}m$) or ordered as the lithium cation in $LiFe_5O_8$ (space group $P4_132$) (9–12). In these iron oxides, a change of the cation-to-anion ratio in the cubic phase leads to a deviation from oxygen stoichiometry, $Fe_{3(1-\delta)}O_4$. δ is directly related to

0022-4596/02 $35.00

the fraction of Fe^{2+} which is oxidized into Fe^{3+}. It can be positive or negative according to the nature of the defects: cationic vacancies ($\delta > 0$) or cation interstitial ($\delta < 0$). In principle, δ could be varied in the spinel phase from negative values to a maximum corresponding to the highest valence of each cation ($\delta_{max} = \frac{1}{9}$ for $Fe_{3(1-\delta)}O_4$). However, the full range of δ has very rarely been investigated for the spinel phase with a given grain size. In room conditions and even in less restricted conditions (temperature lower than 500°C and pO_2 higher than 10^{-5} Pa), the Fe^{2+} cations are not thermodynamically stable and are almost completely oxidized to Fe^{3+}, so that nanometric compounds homogeneous in chemical composition and with $\delta \sim 0$ cannot be investigated in room conditions (13). That is why maghemite ($\delta = \delta_{max}$), rather than magnetite ($\delta = 0$), has been chosen for this study as a model material. In this paper, a range of homogeneous γ-Fe_2O_3 nanoparticles has been prepared by a soft chemistry method using ferrous and ferric chloride salt precipitation. The precipitation was followed by a thermal treatment to eliminate remaining impurities and to reach a stoichiometric state where all Fe cations were oxidized to Fe^{3+} ($\delta = \delta_{max}$). The temperature of this treatment was governed by four parameters: elimination of impurities [water vapor can adsorb molecularly or dissociatively, the latter usually resulting in adsorbed hydroxyl groups on the surface (14)], oxygen stoichiometry of the final product, crystallite size, and transition temperature between γ- and α-Fe_2O_3 [it is well known that γ-Fe_2O_3 is transformed to hematite α-Fe_2O_3 at temperatures between 350°C and 600°C as a function of its previous history (15, 16)]. These parameters have been optimized in order to control the final γ-Fe_2O_3 product. The purpose of the present paper is to investigate the relationships between the vacancies ordering and the lattice parameter in the grain size of γ-Fe_2O_3 samples.

2. EXPERIMENTAL

2.1. Nanoparticles Preparation

Among the numerous methods of nanometer-sized powder synthesis, soft chemistry precipitation has been chosen (17, 18). Synthesis conditions were controlled to obtain powders homogeneous in size and oxygen stoichiometry (19). The preparation was divided into three steps:

(I) Cations precursors, $FeCl_3 \cdot 6H_2O$ and $FeCl_2 \cdot 4H_2O$ (89.40 g and 145.15 g, respectively), were dissolved in 500 ml of an HCl solution (pH < 0.5). Coprecipitation of this mixture with a 28% NH_3 solution was conducted under stirring (700 rpm). The reaction was exothermic so the basic solution was added slowly. Stirring was maintained for 20 min to facilitate the aging process known as Oswald ripening. During all these steps, the temperature was adjusted to ambient, 50°C, 70°C, or 90°C in order to control the size of particles obtained.

(II) The solution was then centrifuged at 3500 rpm. The resulting brown powder was washed with bidistillate water under ultrasonication for 5 min to eliminate chloride impurities. The centrifugation/wash cycle was pursued until "sol" appearence (about four cycles). A freeze-drying process then allowed us to collect a highly divided powder. This method involves solvent extraction under primary vacuum. In this step, solvent was sublimated and was collected by a nitrogen trap between the vacuum pump and sample.

(III) All powders synthesized by the previous methods were submitted to a thermal treatment in order to eliminate remaining impurities and to produce γ-Fe_2O_3 nanoparticles. Under air atmosphere, samples were inserted at room temperature in a tubular furnace, heated at $2°C \cdot min^{-1}$ up to 250°C, and then kept in the furnace for 4 h. Maghemite samples were then cooled slowly to room temperature by shutting off the furnace.

2.2. Characterization of Nanoparticles

The oxidation reaction and impurities departure in precipitate (about 15 mg) were studied by thermogravimetry (SETARAM TAG24). This symmetric thermobalance was able to measure weight variations of 0.1 μg.

Room-temperature XRD patterns were collected on a Siemens D5000 automatic powder diffractometer, operating at 35 mA and 50 kV (20). Fluorescence effects were minimized by using Cu$K\beta$ radiation and correction for instrumental broadening was determined from a standard reference material, annealed BaF_2. Pattern decomposition was carried out by means of both the profile fitting program PROFILE (available in the PC software package DIFFRAC AT supplied by SIEMENS) and the Rietveld method using the XND 1.22 software (21) to obtain parameters defining the position, height, area, integral width, and shape of Bragg reflections. Pseudo-Voight peak profile analysis, using the Langford method (22, 23), was performed to determine both the average crystallite size (size of a region over which the diffraction is coherent) and crystallographic imperfections (microdistorsions, stacking faults, etc.). The powder lattice parameters were deduced from XRD line positions using a least-squares refinement method with in-house software taking into account the effect of sample gap. This technique is used for data analyses in order to obtain reliable lattice parameters despite the effect of sample adjustment on line positions (24).

Surface area measurements have been performed using an AUTOSORB apparatus and 150–200 mg of powder. Samples were outgassed *in situ* at 200°C and the measurements were performed at liquid N_2 temperature with N_2 adsorbing gas. The generalized equation of BET has been used in calculation of surface area values from the isotherm of nitrogen adsorption. The mean apparent particle diameter was inferred from surface area using the equation

ϕ(nm) = 6000/4.86S where S is the surface area ($m^2 \cdot g^{-1}$). TEM characterization, using a Jeol 200CX, has been performed in order to investigate both the shape and the granulometric distribution of the nanoparticles.

For absorbent preparation, maghemite nanoparticles (2 mg) were supported on 100 mg of potassium bromide (KBr). Samples were mixed and ground using an agate mortar and pestle. After grinding, samples were pressed into a disk, of 13 mm diameter, using a pressure of 150 $kg \cdot cm^{-3}$. All spectra were recorded on a Perkin-Helmer 1725X FTIR spectrophotometer.

3. RESULTS AND DISCUSSION

Powders prepared by soft chemistry were characterized by X-ray diffraction and surface area measurements. If the synthesis temperature was higher than 20°C, the spinel phase was obtained directly whatever the temperature (Fig. 1a). Figure 1b shows that a preparation temperature below ambient formed only goethite (α-FeO(OH)) compound. Temperature higher than 20°C is necessary to obtain directly the spinel form. Table 1 gives the evolution of surface areas and lattice parameters versus synthesis temperature of the spinel phase obtained. It shows that surface areas decreases when synthesis temperature increases: temperature provides grain growth rather than germination phenomenon. Although ferric and ferrous chlorides have been dissolved in stoichiometric proportions, large deviations from oxygen stoichiometry relative to significant oxidation of Fe^{2+} cations to Fe^{3+} cations were observed after precipitation. Such an oxidation was quantified by X-ray diffraction from quantitative determination of cell parameters by least-squares refinements (Table 1). All precipitates had a cell parameter equal to about 8.370 Å. This value has to be compared with the lattice parameters of Fe_3O_4 ($\delta = 0$), 8.396 Å, and γ-Fe_2O_3 ($\delta = \frac{1}{9}$), 8.346 Å, which both have the spinel structure. Since the relationship between δ and the cell parameter is approximatively linear (25) a large oxidation of about 65% of the Fe^{2+} cations was then clearly evidenced. During precipitation and immediate characterization under air atmosphere, oxidation of Fe^{2+} cations takes place in crystallites due to their nanometric sizes. As Fe^{2+} cations are not thermodynamically stable in air, a significant amount of Fe^{2+} cations can be oxidized. Such an oxidation phenomenon has been explained on the basis of very significant stresses generated in the crystallites during the oxidation mechanism (26).

TABLE 1
Bulk and Surface Properties of Precipitates[a]

Synthesis temperature (°C)	Amb.	50	70	90
BET surface area ($\pm 1\ m^2 \cdot g^{-1}$)	169	132	116	100
Lattice parameter (± 0.001 Å)	8.368	8.372	8.378	8.377

[a] Surface area was obtained by N_2 coverage measurements and lattice parameter was calculated from the XRD pattern using refinement of line shape position.

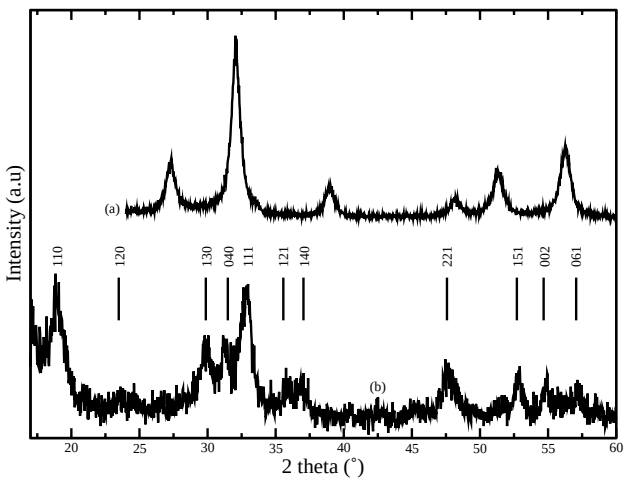

FIG. 1. XRD patterns of (a) $Fe_{3(1-\delta)}O_4$ powder (synthesis temperature 90°C) obtained by soft chemistry and exhibiting the spinel structure lines and (b) goethite α-FeO(OH) powder obtained from low-temperature synthesis (about 0°C and below).

To control elimination of impurities and oxygen stoichiometry of maghemite powders, DTG measurements, under air atmosphere, have been carried out. These measurements show a mass loss (Fig. 2) attributed to the elimination of impurities. The weight change owing to oxidation of Fe^{2+} appears to be negligible compared to the weight loss due to adsorbed water and departure of impurities. The highest mass loss peak at temperature of 20–100°C was consistent with impurities like water physisorbed on surface. For identical mass samples, mass loss was related to crystallite size through surface area: an increase of particle size was accompanied by a decrease of mass loss. Figure 2 shows that at about 250–300°C, mass loss was negligible. Such temperatures were necessary to eliminate remaining impurities. Nevertheless, a compromise between phase transformation (γ- and α-Fe_2O_3) and elimination of impurities must be found. Indeed, the smallest particles (9 nm) showed high reactivity: about 270°C, the hematite compound was detected in samples (Fig. 3a). So, the thermal treatment temperature must be controlled to avoid hematite compound formation: it must be lower than 270°C. Calcination under air at 250°C for 4 hours after a ramp of $2°C \cdot min^{-1}$ have been carried out. During this treatment crystallite growth was negligible as seen by comparison of surface areas of powders before and after calcination (Tables 1 and 2). Table 2 shows that different nanometric particles sizes were obtained as a consequence of the strict control of reactor temperature at the time of coprecipitation. The XRD patterns corresponding to these

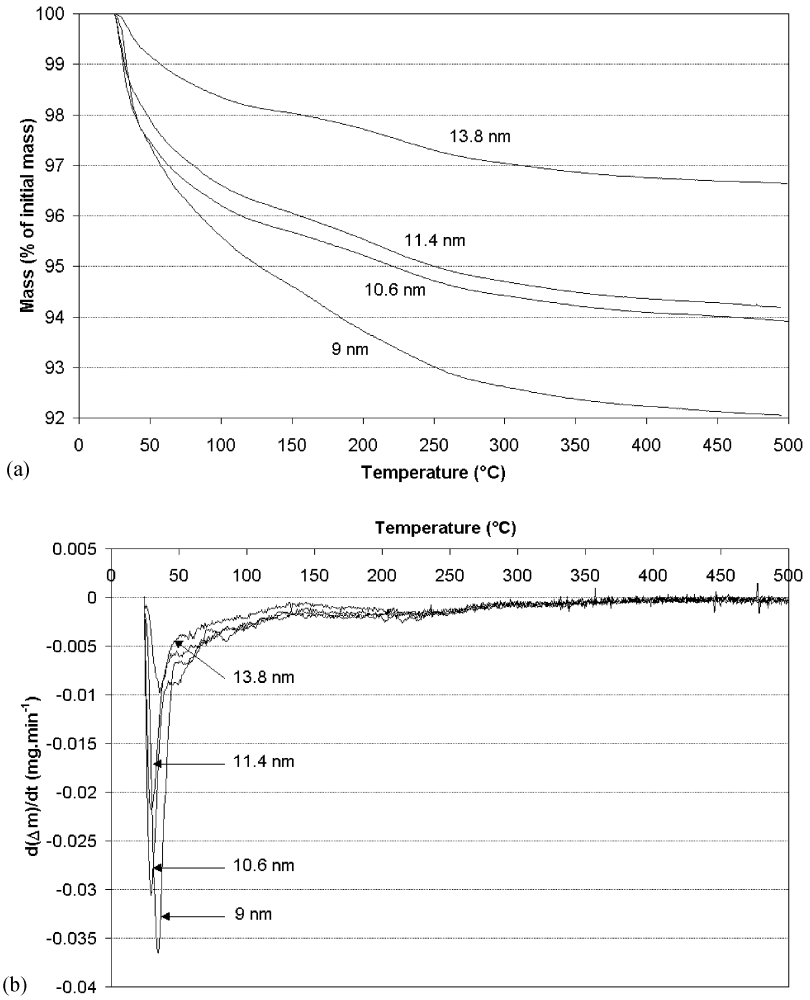

FIG. 2. Thermogravimetric oxidation curves (a) $\%m = f(T)$ and differential curves (b) $d(\Delta m)/dt = f(T)$ of γ-Fe_2O_3 samples obtained by soft chemistry and with crystallite sites of 9, 10.6, 11.4, and 13.8 nm. Air flow was $0.16\,l \cdot min^{-1}$ and temperature ramp $2°C \cdot min^{-1}$.

samples were very similar and could be indexed on the basis of the unit cell corresponding to maghemite crystallized in the $P4_132$ space group (10) (Fig. 3b). No hematite was detected at the resolution device (about 1.5% amount). Moreover, FTIR experiments (Figs. 5 and 6), which are more precise than XRD, did not show α-Fe_2O_3 structural bands (580, 485, 385, 355 cm^{-1}). EELS, XANES, and EXAFS experiments have also been carried out on these powders. The patterns obtained (and not yet published) illustrated only the presence of γ-Fe_2O_3 compound. Cell parameter refinement led to values in relation to the 8.346 Å theoritical value calculated by the Poix method (25). XRD patterns were also consistent with crystalline samples without amorphous phase. Indeed, the background level was so low that the amount of the amorphous compound was negligible. A calculation of this background level has been carried out in our laboratory (taking into account Compton effect, atoms vibrations, etc., but not the amorphous components) and shows results similar to the experimental ones. That was the proof that the amorphous component was negligible. Consequently, there was no particles size below 5 nm which confirmed the narrow crystallite size distribution (1). Nitrogen BET measurements shows surface area ranging from 133 to 89 $m^2 \cdot g^{-1}$ (Table 2). TEM microscopy (Figs. 4a and 4b) illustrates a narrow particle size distribution and spherical shape. Moreover, the major proofs of the narrow size distribution of our powders were both the symmetrical line profile of each diffraction peaks (27) and the shape factor of this line profile which was intermediate between 0.6466 and 0.9394 (for example, 0.729 for the (511) peak). If our products had a wide size distribution, a Lorentzian profile would be obtained. According to the Langford method, the peak broadening was due only to size effects: after the thermal treatment under air atmosphere at 250°C, a range of nanoparticles from 9 to 14 nm was obtained with a controlled stoichiometry similar to that of the maghemite

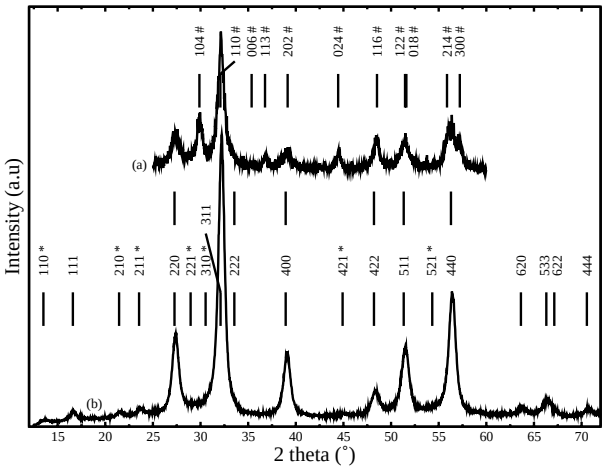

FIG. 3. Powder XRD pattern of the Fe_2O_3 sample, obtained by soft chemistry, containing (a) maghemite and hematite (#) phases after thermal treatment at 270°C for 4 hours in air and (b) maghemite γ-Fe_2O_3 sample obtained at 250°C for 4 hours in air. All peaks are indexed and asterisks illustrate vacancies ordering.

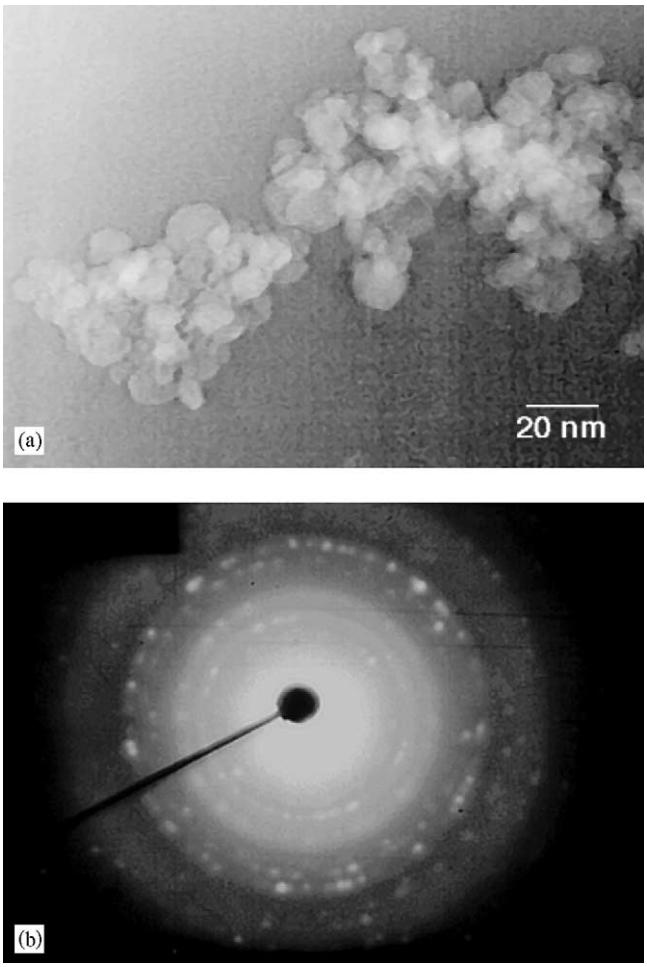

FIG. 4. (a) Bright-field image of the spherical shape nanocrystalline γ-Fe_2O_3 sample, obtained by soft chemistry, after thermal treatment at 250°C for 4 hours in air with its corresponding SAD pattern (b) which shows good crystallization. This sample has an average crystallite size of 15 mn and surface area of about 89 $m^2 \cdot g^{-1}$.

compound (Table 2) and without crystallographic imperfections. These observations show that it is possible to control crystallite growth for the γ-Fe_2O_3 oxide. Now it is essential to provide evidence for the crystallinity and the purity of these products.

Infrared spectra of the γ-Fe_2O_3 nanoparticles have been reported (Fig. 5) to show the absence of chloride impurities after thermal treatments. In Figs. 5a and 5b, some noticeable absorption bands appeared, even after thermal treatment, at ~ 3400, 1640, and in the 800–400 cm^{-1} region. The high-frequency bands (3400 and 1640 cm^{-1}) were assigned to hydroxide and water, respectively, on the maghemite surface. Low-frequency bands (800–400 cm^{-1}) were assigned to spinel γ-Fe_2O_3 structure. Interpretation of these two bands has been proposed by R. D. Waldron (28) and W. B. White (29): v_1 band (580 cm^{-1}) refers to Fe–O deformation in octahedral and tetrahedral sites while v_2 band (420 cm^{-1}) refers only to Fe–O deformation in octahedral sites. The 900–1400 cm^{-1} bands on the precipitate spectrum (Fig. 5a) showed the presence of impurities like chlorides. After thermal treatments, these bands disappeared and additional substructures bands (730, 696, 636, 560, 482, and 442 ± 2 cm^{-1}) were visible on the enlargement of the infrared spectrum at the lowest wavenumbers (Fig. 6). These well-resolved absorption bands were due to the ordered spinel structure which exhibits a larger number of IR bands than the disordered material (29, 30).

Vacancies in the γ-Fe_2O_3 compound could be ordered as previously stated in the introduction (31). The ordering scheme adopted by γ-Fe_2O_3, like $LiFe_5O_8$, depends on both the crystallite size and synthesis route (9). It was suggested that vacancies ordering changes the symmetry of the spinel phase (cubic $Fd\bar{3}m$ to tetragonal $P4_12_12_1$) (28) or appears without any distortion of cubic cell (cubic $Fd\bar{3}m$ to cubic $P4_132$) (12). This change in symmetry (space group: $Fd\bar{3}m$ to

TABLE 2
Bulk and Surface Properties of Nanometric γ-Fe_2O_3 Powders[a]

Synthesis temperature (°C)	Amb.	50	70	90
BET surface area (± 1 $m^2 \cdot g^{-1}$)	133	116	108	89
Particles diameter (± 1 nm) deduced from surface area measurements	9.3	10.6	11.4	13.8
Lattice parameter (± 0.001 Å)	8.347	8.349	8.347	8.346
Particles diameter (XRD data) (± 2.0 nm)	8.4	9.2	10.7	12.3

[a] Surface area was obtained by N_2 coverage measurements and used to determine particle diameter. Lattice parameters were calculated from XRD pattern using refinement of line shape position.

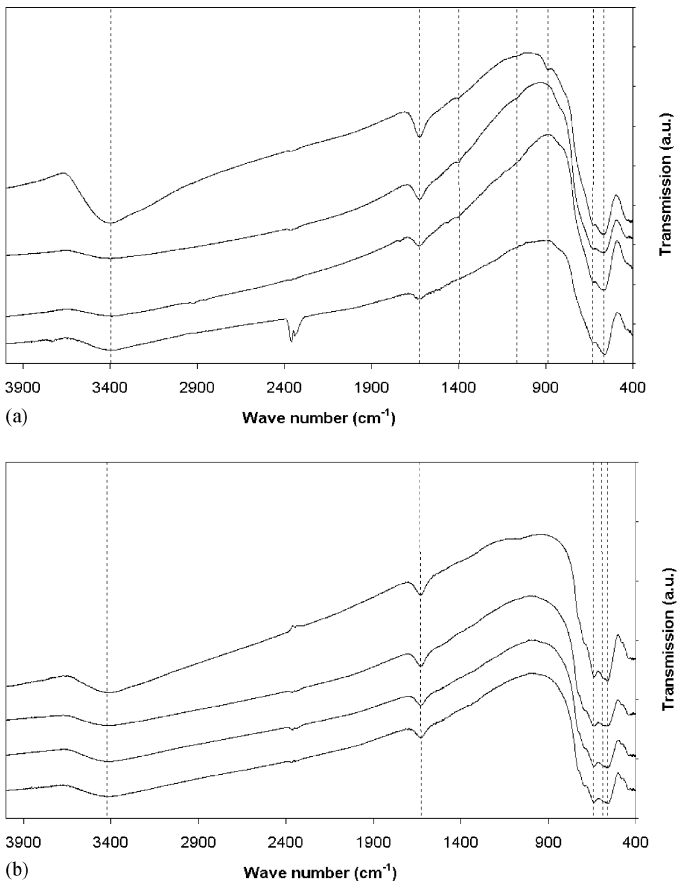

FIG. 5. Infrared spectrums of maghemite nanoparticles supported on potassium bromide (a) before and (b) after thermal treatment at 250°C for 4 hours showing the presence of hydroxide (3400 cm^{-1}) and water (1640 cm^{-1}), appearance of γ-Fe_2O_3 structure bands (< 800 cm^{-1}), and departure of some impurities such as chloride (900–1400 cm^{-1}). From bottom to top, spectrum (a) and (b) 9, 10.6, 11.4, and 13.8 nm.

$P4_132$) induces additional bands particularly in the well-resolved high-frequency triad at 700–500 cm^{-1}. In the literature, these additional bands were reported to disappear for crystallite size lower than 10 nm (29); that was not the case here. The vacancies in γ-Fe_2O_3 particles synthesized in this study were not distributed at random. With resonant XRD and neutron diffraction experiments we have shown that the vacancies were in the octahedral position (32, 33).

Figure 7 shows the lattice parameter variation with crystallite size of γ-Fe_2O_3 reported in the literature (1) and in the case of the well-controlled maghemite particles of the present study. The crystallite size modification of our products does not induce lattice parameter variation. A similar result has been obtained for controlled titanium ferrite $Fe_{2.5}Ti_{0.5}O_4$ in the 8–60 nm range (33). The lattice parameter variation in the 8.346–8.396 Å range observed by Ayyub *et al.* (1) may be rather due to the lack of control of the deviation from oxygen stoichiometry of their products. Indeed, 8.396 Å is the lattice parameter of magnetite and

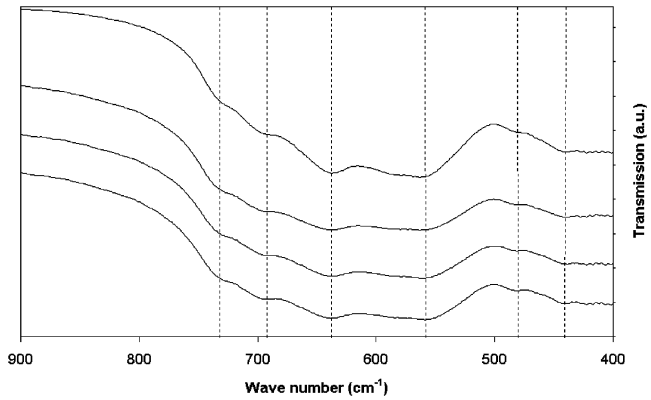

FIG. 6. Enlargement of infrared spectra of maghemite nanoparticles supported on potassium bromide after thermal treatment at 250°C for 4 hours showing substructure bands of maghemite. These bands confirmed the crystallinity of samples even at about 9 nm crystallite size. From bottom to top: 9, 10.6, 11.4, and 13.8 nm.

8.346 Å is that of maghemite. Such a variation may be also due to the vacancy ordering (in tetrahedral or octahedral coordination). Figure 7 shows that in the range 9–14 nm maghemite with controlled vacancy ordering, oxygen stoichiometry, and surface cleanness does not show any lattice parameter variation (8.347 ± 0.002 Å for all these powders). In the same way, the evolution of the lattice parameter observed on $BaTiO_3$ samples (3–5) has been explained by the lack of control of hydroxide amount in these powders treated at different temperature (34). So for the γ-Fe_2O_3 model materials studied here and in the particle size range (9–14 nm), the cell parameter appears to be not linked to crystallite size. However, Hansen *et al.* (35) demonstrated in the case of nanometric metal particles that there were very small changes in bond length with particle size. It was found that there was a tendency for the distance

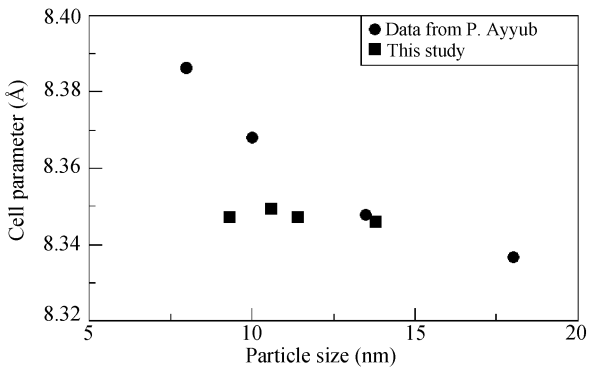

FIG. 7. Correlation between the cell parameter (cubic) and the XRD particle size in γ-Fe_2O_3 nanoparticles. The variations observed from P. Ayyub's data (1) may be due to the lack of control of the material's chemical composition. In this study, cell parameters do not vary significantly with crystallite size (stoichiometry and cleanness are controlled).

between the first and the second layers to contract of 2.5–4.5%. This effect was seen in the 0.8–10 nm range. Moreover, on our γ-Fe_2O_3 model nanoparticles, studies of water adsorption that we have not yet published show small changes in lattice parameter versus surface coating. In conclusion, the surface has a small influence on the lattice parameter but only in the case of water adsorption or for the first atomic layers.

4. CONCLUSION

A size-fixed range of maghemite nanoparticles γ-Fe_2O_3 has been synthesized by a soft chemistry route using precipitation of chloride salts in stoichiometric proportions. Varying synthesis temperatures lead to different sizes of nanoparticles from 9 to 14 nm. In order to obtain highly divided powder, centrifugation and freeze-drying processes have been used before thermal treatment at 250°C under air atmosphere. X-ray diffraction and surface area measurements confirmed the nanometric scale. TEM and XRD showed both their narrow size distribution and their spherical shape. Absorption bands in IR spectra were assigned to hydroxide, water, and maghemite structure. Substructure bands were observed even at 9 nm showing the perfect crystallographic order of ions and vacancies. No impurities were revealed after thermal treatment. For these model materials and in this crystallite size range, particles size does not influence lattice parameter. The lattice parameter variation (8.346–8.396 Å) range observed by Ayyub *et al.* (1) may rather be due to the lack of control of the deviation from oxygen stoichiometry of their products or of the vacancy ordering. The effect of surface stress on lattice parameter appears to be negligible in the 9–14 nm range.

ACKNOWLEDGMENTS

The authors thank Prof. C. Esnouf for TEM experiments and Prof. P. Perriat, both in GEMPPM Laboratory in INSA of Lyon, for helpful discussions.

REFERENCES

1. P. Ayyub, M. Multani, and M. Barma, *J. Phys. C, Solid State Phys.* **21,** 2229–2245 (1988).
2. J. L. Dormann, D. Fiorani, and E. Tronc, *Adv. Chem. Phys.* **98,** 283 (1997).
3. N. Bernaben, A. Leriche, B. Thierry, J. C. Niepce, and R. Waser, *Fourth Euro Ceram.* **5,** 203–210 (1995).
4. G. Caboche, F. Chaput, J. P. Boilot, and J. C. Niepce, *Silicates Ind.* **5,** 103 (1993).
5. S. Malbe, J. C. Mutin, and J. C. Niepce, *J. Chem. Phys.* **80,** 825 (1992).
6. P. Perriat, *Nanostruct. Mater.* **6,** 791–794 (1995).
7. P. Perriat and J. C. Niepce, *High Temp. Chem. Processes* **3,** 585–600 (1994).
8. C. Laberty and A. Navrotsky, *Geochim. Cosmochim Acta* **62,** 2905–2913 (1998).
9. M. P. Morales, C. Pecharroman, and T. Gonzalez-Carreno, *J. Solid State Chem.* **108,** 158–163 (1994).
10. M. P. Morales, M. Andres-Verges, S. Veintemillas-Verdaguer, M. I. Montero, and C. J. Serna, *J. Magn. Magn. Mater.* **203,** 146–148 (1999).
11. C. Greaves, *J. Solid State Chem.* **49,** 325–333 (1983).
12. A. N. Shmakov, G. N. Kryukova, and S. V. Tsybulya, *J. Appl. Crystallogr.* **28,** 141–145 (1995).
13. N. Guigue-Millot, Y. Champion, M. J. Hÿtch, F. Bernard, S. Bégin-Colin, and P. Perriat, *J. Phys. Chem. B* **105,** 7125–7132 (2001).
14. Y. Joseph, C. Kuhrs, and W. Ranke, *Chem. Phys. Lett.* **314,** 195–202 (1999).
15. E. Herrero, M. V. Cabanas, and M. Vallet-Regi, *Solid State Ionics* **101–103,** 213–219 (1997).
16. G. Ennas, G. Marongiu, and A. Musinu, *J. Mater. Res.* **14,** 1570–1575 (1999).
17. N. Millot, S. Begin-Colin, and P. Perriat, *J. Solid State Chem.* **139,** 66–78 (1998).
18. J. P. Jolivet, "De la solution à l'oxyde." Inter Editions, CNRS Editions, Paris, 1994.
19. P. Cousin and R. A. Ross, *Mater. Sci. Eng. A* **130,** 119–125 (1990).
20. M. Oetzel and G. Heger, *J. Appl. Crystallogr.* **32,** 799–807 (1999).
21. J. F. Berar and G. Baldinozzi, *IUCR-CPD Newsl.* **20,** 3–5 (1998).
22. J. I. Langford, National Institute of Standards and Technology, Special Publication, 846, pp. 110–126. NIST, Washington, DC, (1992).
23. N. C. Halder and C. N. J. Wagner, *Acta Crystallogr.* **20,** 91–106 (1966).
24. F. Bernard, F. Charlot, and P. Sarrazin, *J. Phys. IV* **6,** 103–110 (1996).
25. P. Poix, "Liaisons interatomiques et propriétés physiques des composés minéraux." Suchet, Paris, 1966.
26. P. Perriat, B. Domenichini, and B. Gillot, *J. Phys. Chem. Solids* **57,** 1641 (1996).
27. J. I. Langford, D. Louër, and P. Scardi, *J. Appl. Crystallogr.* **33,** 964–974 (2000).
28. R. D. Waldron, *Phys. Rev.* **99,** 1727–1735 (1955).
29. W. B. White and B. A. DeAngelis, *Spectrochim Acta* **23A,** 985–995 (1967)
30. B. Gillot, *Vibrat. Spectrosc.* **6,** 127–148 (1994).
31. K. Haneda and A. H. Morrish, *Solid State Commun.* **22,** 779–782 (1977).
32. F. Bernard, J. Lorimier, V. Nivoix, N. Millot, P. Perriat, B. Gillot, J. F. Berar and J. C. Niepce, *J. Solid State Chem.* **141,** 105–113 (1998).
33. N. Guigue-Millot, Thesis, University of Burgundy, 1998.
34. F. Perrot-Sipple, Thesis, University of Burgundy, 1999.
35. L. B. Hansen, P. Stoltze, and J. K. Norskov, *Phys. Rev. Lett.* **64,** 3155–3158 (1990).